ADVANCED FUNCTIONAL MATERIALS
www.afm-journal.de

Intermolecular Interactions as Driving Force of Increasing Multiphoton Absorption in a Perylene Diimide-Based Coordination Polymer

Simon Nicolas Deger, Anna Mauri, Yang Cui, Sebastian Josef Weishäupl, Ali Deniz Özdemir, Hamad Syed, Aleksandr Ovsianikov, Wolfgang Wenzel, Alexander Pöthig, Jürgen Hauer, Mariana Kozlowska,* and Roland Augustinus Fischer**

Coordination polymers (CPs) represent an innovative class of materials with proven potential for multiphoton absorption applications. However, understanding the structure-property relationships that govern their nonlinear optical behavior remains challenging. This study presents an in-depth investigation of the effects of intermolecular interactions on multiphoton absorption by focusing on the synthesis and characterization of 1,6,7,12-tetrachloroperylenediimide-N,N'-di-(acetic acid) (H_2tpda) and its coordination with zinc to form [Zn_2tpda$(DMA)_2(DMF)_{0.3}$] (Zntpda). How the packing of tpda linkers within the coordination framework influences their optical properties is revealed. The analysis demonstrates that Zntpda exhibits a broadened UV–vis absorption spectrum with no emission indicative of H-type aggregation with additional evidence of a photo-induced electron transfer. Z-scan measurements show enhanced two-photon absorption (2PA) cross-sections of Zntpda compared to H_2tpda and even three-photon absorption (3PA). This is explained by intermolecular interactions, electronic coupling, and spatial confinement effects within the polymer. The findings underscore the critical role of chromophore orientation and packing in optimizing nonlinear optical performance, offering insights for designing advanced functional CP materials tailored for photonic applications.

1. Introduction

Supramolecular chemistry comprises the arrangement of molecules via intermolecular interactions to form structures of higher complexity.[1] The implementation of molecules into supramolecular assemblies can go along with significant changes in their properties and functionalities, offering valuable insights into the behavior of such materials and potential avenues to steer their properties and enable desired applications.[2] In this context, perylene-3,4:9,10-tetracarboxylic acid diimide (PDI) based chromophores have been proven to be versatile building blocks.[3]

The PDI chromophores offer favorable properties stemming from their chemical structure: a rigid polycyclic aromatic scaffold substituted with two dicarboxylic acid imide groups and strong conjugation between the electron-rich perylene core and the electron-withdrawing imide groups.[3] The resulting characteristics

S. N. Deger, S. J. Weishäupl, A. Pöthig, R. A. Fischer
Technical University of Munich
TUM School of Natural Sciences
Department of Chemistry
Chair of Inorganic and Metal–Organic Chemistry
Catalysis Research Center
Lichtenbergstraße 4, 85747 Garching, Bavaria, Germany
E-mail: roland.fischer@tum.de

A. Mauri, A. D. Özdemir, W. Wenzel, M. Kozlowska
Institute of Nanotechnology (INT)
Karlsruhe Institute of Technology (KIT)
Kaiserstr. 12, 76131 Karlsruhe, Baden-Württemberg, Germany
E-mail: mariana.kozlowska@kit.edu

Y. Cui, J. Hauer
Technical University of Munich
TUM School of Natural Sciences
Department of Chemistry
Professorship for Dynamic Spectroscopy
Catalysis Research Center
Lichtenbergstraße 4, 85747 Garching, Bavaria, Germany
E-mail: juergen.hauer@tum.de

H. Syed, A. Ovsianikov
Research Group 3D Printing and Biofabrication
Institute of Materials Science and Technology
Technische Universität Wien (TU Wien)
Getreidemarkt 9, Vienna 1060, Austria

The ORCID identification number(s) for the author(s) of this article can be found under https://doi.org/10.1002/adfm.202424656

DOI: 10.1002/adfm.202424656

include comparably high thermal, chemical, and photochemical stability, broad absorption spectra, fluorescence with high quantum yields, and flexibility for various structural modifications.[3,4]

These properties have led to their application in various supramolecular material classes, encompassing pure organic dimers,[5] catenanes,[6] and macrocycles,[7] as well as metal–organic supramolecular assemblies such as metal–organic polyhedra (MOPs),[8] and coordination polymers (CPs),[9] along with their subgroup Metal–Organic Frameworks (MOFs).

CPs and MOFs comprise organic linker molecules, forming coordination bonds with metal-based secondary building units (SBUs). PDI-based linkers have already been incorporated into CPs and MOFs to impart their properties to the materials, enhancing or enabling their performance in the respective applications. These applications span photocatalysis,[10] photothermal conversion,[11] electrical conductivity,[12] energy transfer,[13] gas separation,[14] and singlet oxygen evolution.[15] PDI molecules have been extensively explored in the field of nonlinear optics (NLO),[16] including multiphoton absorption (MPA), a phenomenon with applications in bioimaging (such as in medical imaging techniques), 3D-data storage (e.g. in advanced computer memory systems), and microfabrication (for creating intricate structures at a microscale).[17] Despite these recent advances, the impact of assembling PDI chromophores in MOFs for MPA applications has yet to be explored.[17]

The generally high potential of CPs/MOFs for MPA has already been demonstrated, as different MPA active chromophore linkers have already been incorporated in these materials, predominantly leading to an improvement in two-photon absorption (2PA) cross-section $\sigma^{(2)}$. This system property has the unit of Göppert–Mayer (GM = 10^{-50} cm^4 × s × photon^{-1}) and can be used to quantify the MPA activity.[17,18] The observed increase of the 2PA cross-section upon insertion of an organic linker into a CP can be attributed to different effects: (I) rigidity enforced by the framework reducing radiation-less decay pathways, (II) increased stability through a reduction in photobleaching, (III) polarization by the metal node and (IV) intermolecular interactions between the packed chromophores.[17,19] The latter has been postulated to contribute significantly to the aforementioned increase in $\sigma^{(2)}$, as supramolecular self-assembly effectively shortens the distance between organic conjugated monomers. This facilitates abundant intermolecular interactions such as π-π and hydrogen bonds in the molecular crystal, promoting the electronic coupling between monomer molecules and enhancing the degree of electron delocalization between monomer molecules in the crystal, promoting charge transfer (CT).[18c,20] However, these effects have only been studied sparsely in the reports on MPA in MOFs.[21] In purely organic systems, the aggregation-induced enhancement of MPA has already been investigated in several studies, showing that intermolecular interactions, as well as the orientation of dipole moments, are contributing factors in the improvement of $\sigma^{(2)}$.[22] This knowledge can be potentially transferred to the arrangement of chromophores in MOFs.

Herein, we report our related efforts, presenting the synthesis of a new PDI-based CP using 1,6,7,12-tetrachloroperylenediimide-N,N'-di-(acetic acid) (**H_2tpda**) and $Zn(NO_3)_2$ × 6 H_2O. Single-crystal X-ray diffraction (SC-XRD) revealed the structure to be a 1D CP with the composition [Zn_2tpda(DMA)$_2$(DMF)$_{0.3}$] (**Zntpda**). Following the structural characterization of the CP, the photophysical properties of both the linker and the CP were analyzed and compared, revealing emission quenching in the CP due to aggregation-caused quenching (ACQ), probably originating from a photo-induced electron transfer (PET) and H-type aggregation. MPA of both the linker and the CP were investigated and compared, revealing a drastic increase of $\sigma^{(2)}$ and the occurrence of comparatively high three-photon absorption (3PA) when the linker is incorporated into the CP. This increase in $\sigma^{(2)}$ was further studied using density functional theory (DFT) and time-dependent (TD) DFT calculations, revealing molecular insights of experimental observations and hinting toward intermolecular interactions as well as rigidification working cooperatively together as a contributing factor in the increase of $\sigma^{(2)}$. These results provide a step toward a better understanding of MPA in MOFs and elucidate the role of intermolecular interactions. This can lead to optimized materials and more straightforward implementation of MOFs and CPs in MPA-related applications.

2. Results and Discussion

2.1. Synthesis and Characterization

The PDI-based chromophore 1,6,7,12-tetrachloroperylenediimide-N,N'-di-(acetic acid) (**H_2tpda**) was synthesized in a two-step synthesis starting from 3,4,9,10-perylene-tetracarboxylic-3,4:9,10-dianhydride, further details can be found in the Supporting Information. Compared to unsubstituted PDI linkers, the chlorine substitution enhances the solubility of **H_2tpda** due to the induced twist of the π-system, facilitating the MOF formation.[15] Additionally, the chlorine substitution enhances the electron density of the chromophore.[23]

The reaction of **H_2tpda** with $Zn(NO_3)_2$ × 6 H_2O in a DMF/H_2O mixture at 120 °C yielded dark red crystals with the composition [Zn_2tpda(DMA)$_2$(DMF)$_{0.3}$] (**Zntpda**, **Figure 1**). The 1D framework crystallizes in the monoclinic space group $P\,2_1/c$ with the unit cell parameters a = 18.7419(19) Å, b = 9.5896(9) Å, c = 20.181(2) Å, and α = 90°, β = 113.328(3)°, γ = 90°. It comprises a $Zn_2O_4N_2$ SBU (Figure 1c) connecting four **tpda** linker motifs and two DMA molecules formed in situ in the reaction solution. Two carboxylic groups bridge the two zinc atoms, which are both tetrahedrally coordinated, in a κ^1:κ^1 mode, and the other two carboxylic groups are connected in a κ^1 mode in the same plane. One dimethylamide (DMA) molecule completes the SBU at each zinc atom on opposite sides of the carboxylic acid plane (Figure 1c). The SBU-connected linker molecules consequently form strings of coordination polymers, each consisting of a double chain of linkers forming a 2-nodal net with 2,4-c net topology (Figure 1a,e).[24] These consequently form layers that are connected by π-interactions. The π-stacked layers of **tpda** molecules alternate between non-inversed and 180° rotated stacks, showing an x-shaped structure along the c-axis (Figure 1f). The linkers in these chains are packed at a distance of 4.44 Å and the following string at a distance of 4.18 Å, resulting in two different dimers **dimer A** and **dimer B** in the structure (Figure 1g,h). The chlorine substitution-induced twisting of the perylene core leads to an off-center slipped stacking of the chromophores in the solid state, similar to other purely organic systems (Figure 1d).[25]

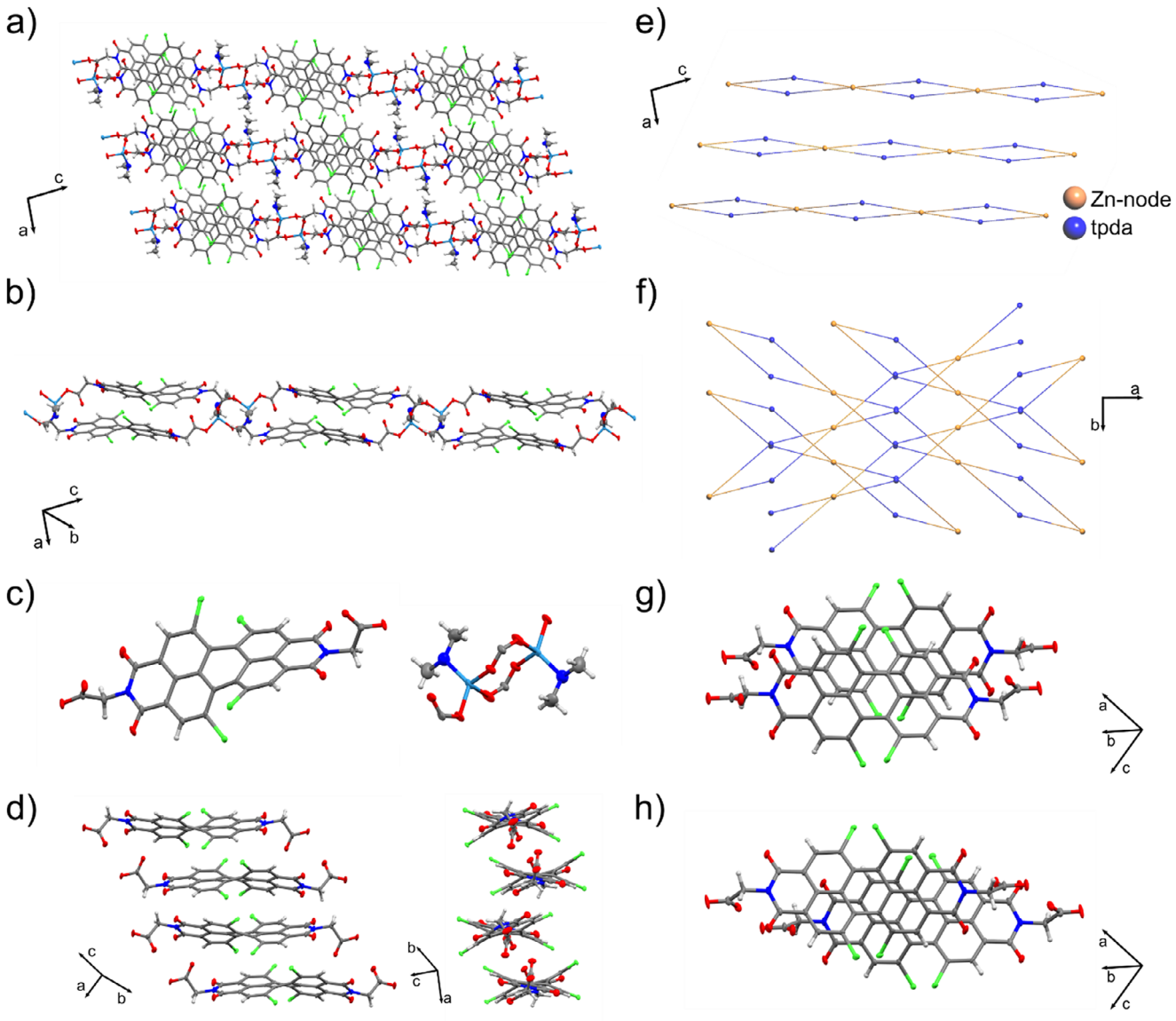

Figure 1. a) Depiction of **Zntpda** along the b-axis showing the linker-SBU-strings. Structure information: $P\,2_1/c$ with the unit cell parameters a = 18.7419(19) Å, b = 9.5896(9) Å, c = 20.181(2) Å and $\alpha = 90°$, $\beta = 113.328(3)°$, $\gamma = 90°$ and R-value = 9.78% b) Depiction of a cut out of **Zntpda** showing a single, double strand of the CP c) Molecular structure of SBU and linker inside the framework. d) Packing of the linkers shown in two directions, visualizing the offset slipped stacking of the chromophores. e) Schematic representation of the underlying network topology along the b-axis. f) Schematic representation of the underlying network topology along the c-axis, highlighting the x-shaped packing of the π-stacked double strand. g) Dimer formed by π-stacking bound linkers of two chains (**dimer A**). h) Dimer formed by the SBUs connected chains (**dimer B**). The angle between the planes of the linkers in **dimer A** and **dimer B** is 96.42° and 58.23°, respectively (see Figure S15, Supporting Information). Color coding: gray = carbon, blue = nitrogen, red = oxygen, green = chlorine, and petrol = zinc.

The phase purity of the bulk of **Zntpda** was investigated by powder X-ray diffraction (PXRD, Figure S5, Supporting Information), which matches the results from SCXRD and elemental analysis (EA). The compound is thermally stable up to 350 °C shown by thermogravimetric analysis (TGA; Figure S7, Supporting Information), and infrared (IR) spectroscopy shows the expected bands for coordinated **tpda** (Figure S6, Supporting Information). In combination, PXRD, EA, and IR prove the successful incorporation of **H_2tpda** in the framework of **Zntpda** and show the sufficient purity of the bulk for the optical characterization.

2.2. Steady-State Optical Analysis

With the synthesized compounds, we conducted steady-state optical measurements. The UV–vis spectrum of **H_2tpda** in THF shows an absorption band with a maximum of 513 nm. As is typically known for perylenes, the absorption spectrum is modulated by a pronounced vibronic progression with the second strongest peak at 481 nm (see black line in **Figure 2**a). Time-dependent and time-independent density functional theory calculations (TD-DFT and DFT, respectively), considering the

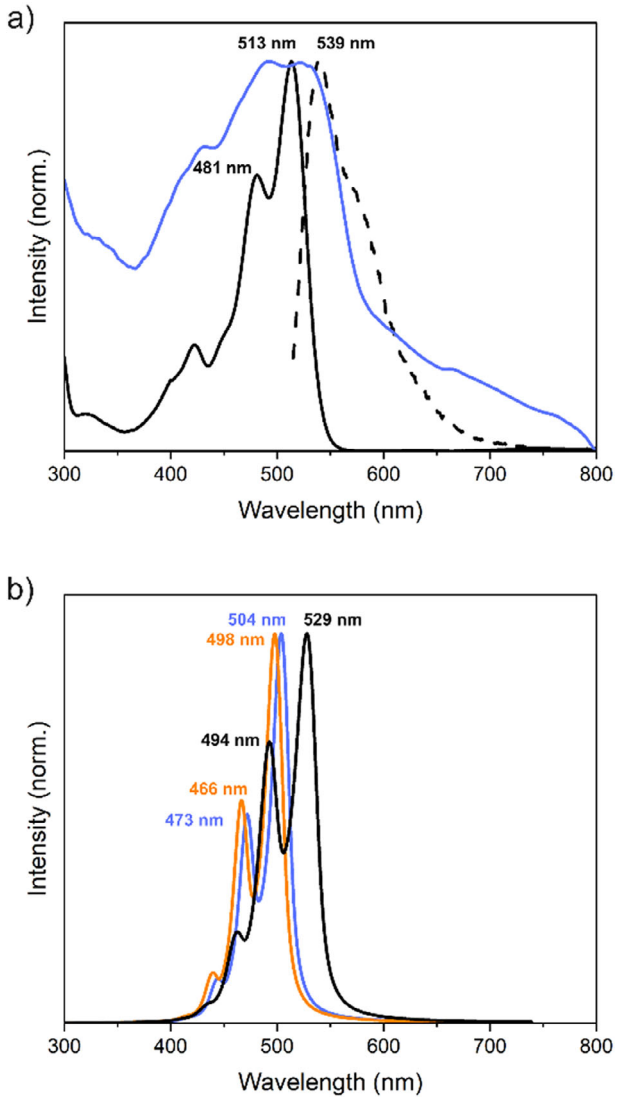

Figure 2. a) UV–vis (black), emission spectra (dotted) of **H_2tpda** in THF, and diffuse reflectance spectrum of **Zntpda** (blue). b) Vibrationally resolved absorption spectra of **H_2tpda** (black), **dimer A** (blue), and **dimer B** (orange) computed with a time-independent FC-TI-LCM approach. Values of transition dipole moments (TDM) and transition quadrupole moments (TQM) are reported in Tables S8 and S9 (Supporting Information) and depicted in Figure S22 (Supporting Information). The comparison to the TD-DFT spectra is depicted in Figure S17 (Supporting Information).

implicit THF solvent and vibronic effects, reproduced the main transitions with peak maxima at 513 (529) nm and 481 (494) nm, respectively (see Figure 2b; Figure S17, Supporting Information). (Note: including vibrational contribution was a prerequisite for the correct absorption calculation of **H_2tpda** (see Figure S16, Supporting Information for comparison)).

Zntpda shows a strongly broadened absorption spectrum compared to **H_2tpda** (see Figure 2a, blue vs. black line). The red-shifted features in the **Zntpda**-spectrum (shoulder between 600 and 800 nm) indicate ground-state interactions between linkers in the CP. The second vibronic peak – located at 481 nm in **H_2tpda** – shows a clear blue shift in the CP. As PDIs are well known for their propensity to form aggregates, this hypsochromic shift is readily explained by H-type aggregation.[26] This is also reflected by the close π-stacked **tpda** molecules in the CP structure, i.e. at a distance of 4.18 to 4.41 Å in our case, with the smallest distances between the planes approaching 3.57 Å. Additionally, the angle between the single chromophores is 96.42° and 58.23° for **dimer A** and **dimer B**, respectively, and angles higher than 54.7° are typically known for H-type aggregates.[27] The indication of such an assembly in **Zntpda** has also been observed in calculated vibrationally-resolved spectra of the two dimer types of **H_2tpda** formed in **Zntpda** (Figure 2b). Here, the blue shift of 25–30 nm upon dimer formation is noticeable. However, the CP formed in the experiment comprises a more complex assembly structure beyond the employed dimer model.

The emission spectrum of **H_2tpda** (dashed black line in Figure 2a) peaks at 539 nm with a small Stokes shift of 24 nm and a fluorescence quantum yield (QY) of Φ = 88%, while **Zntpda** shows no observable emission. This lack of observable fluorescence points again toward the presence of H-type aggregation.[3,26a] Alternatively, the lack of emission can also be explained by the possibility of the PET between **tpda** linkers due to the overlap of the respective frontier orbitals.[28] The electronic coupling between linkers in **dimer A** and **dimer B** is 14.6 meV and 53.5 meV considering the overlap of their highest occupied molecular orbitals (HOMO), and 77.2 meV and 47.6 meV for the lowest unoccupied molecular orbitals (LUMO), respectively, visualized in Figure S21 (Supporting Information). This indicates the possibility of the CT states in the material, as already discussed for other PDI assemblies, which is known to cause the emission quenching.[29]

2.3. Multiphoton Absorption

*2.3.1. Characterization of the Linker **H_2tpda** by Nonlinear Fourier-Transform Spectroscopy*

Nonlinear optical characterization of **H_2tpda** was conducted via nonlinear Fourier-transform spectroscopy (see details in SI) based on two-photon induced fluorescence excitation.[30] The respective 2PA spectrum is presented in **Figure 3a**. **H_2tpda**, as an approximately centrosymmetric molecule, shows a 2PA spectrum in which the 1PA-allowed $S_0 \rightarrow S_1$ transition is missing due to selection rules.[31] Therefore, for wavelengths longer than 864 nm, the $\sigma^{(2)}$-values only reach up to 5 GM. In the 750–820 nm spectral range, the $\sigma^{(2)}$-values approach 24 GM and 98 GM at 719 nm (Figure 3a). This increase in $\sigma^{(2)}$ is caused by the resonance enhancement of 2PA through decreased detuning from the energy of the 1PA transition, as reported previously.[32] In this regard, our results match the spectral characteristics of PDIs with chlorine substituted at the bay position. We note that substitution on the end positions weakly influences the photophysical properties.[23,33] A similar observation can be made in the calculated 2PA spectra of **H_2tpda** (see Figure S19 and Table S2, Supporting Information). The $S_0 \rightarrow S_1$ transition is close to an optically dark transition with a cross-section value of 0.06 GM. The excitations to the S_2 and S_3 are markedly stronger with cross-sections of 0.52–2.78 GM. This is caused by the absence of at least

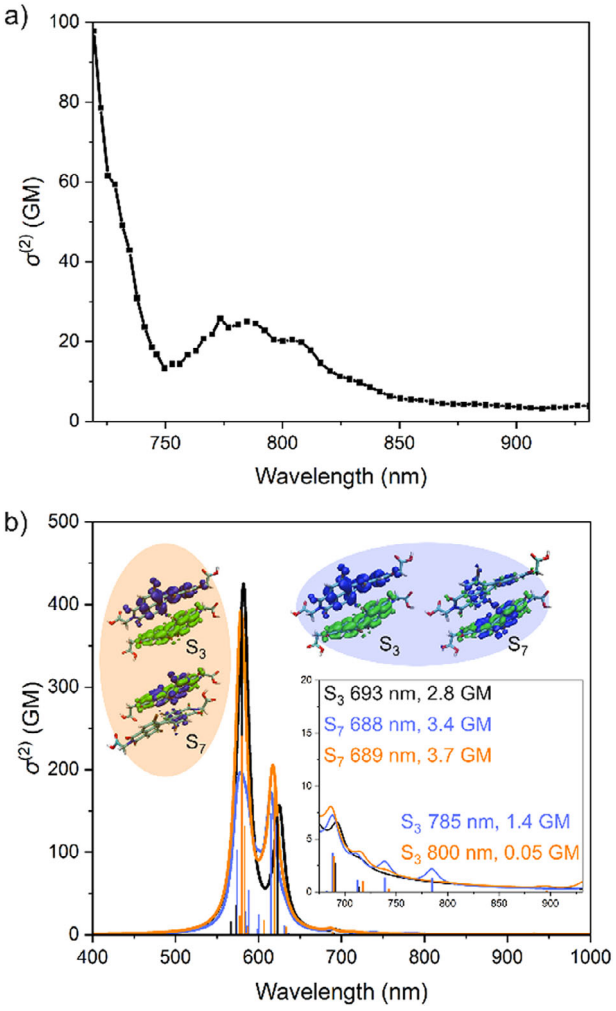

Figure 3. a) Experimental 2PA spectrum of **H_2tpda** in THF. b) Calculated 2PA spectra of **H_2tpda** (in *implicit* THF, COSMO model) (black), **dimer A** (blue), and **dimer B** (in the gas phase) (orange) with the inset of the 650–850 nm range. The electron density difference upon specific excitations is visualized for **dimer A** and **dimer B** in blue and orange ellipsoids, respectively. The electron-donating and accepting regions are visualized in blue and green (isovalue of 0.003 a.u.).

two symmetrically similar 1PA dark states of **H_2tpda**, as the 1PA is rather intense.[22d] Therefore, the 2PA transition does not reach the same final state as the one-photon transition.[32d] It should be noted that the calculated 2PA cross-section values should not be compared directly with the values from the experiment. The cross-section values are sensitive to various experimental parameters and referencing methods. Moreover, the calculated values were not rescaled in comparison to fluorescein, and it is known that cross sections may be underestimated in TD-DFT.[34]

2.3.2. Characterization of the CP *Zntpda* by Z-Scan Measurements

Due to the lack of fluorescence in **Zntpda**, its NLO properties were characterized using the open-aperture Z-scan technique[35] based on transmission measurements at different distances from the beam focus. MPA coefficients can be extracted by fitting the measured Z-scan traces (see details in the Supporting Information). Thus, the Z-scan technique can be applied to characterize non-emissive samples. In the excitation range of the employed femtosecond oscillator from 700 to 950 nm, we observed 2PA in the wavelength range of 700–850 nm (**Table 1**). **Zntpda** shows high $\sigma^{(2)}$-values of up to 62 095 GM at 730 nm. The increase of the 2PA cross sections and the contribution of several close-lying excited states are also noticeable in the TD-DFT calculated spectra of two dimer species extracted from the crystal (see Figure 3b; Tables S3 and S4, Supporting Information). The effect depends on the dimer type, but both show a similar 2PA forbidden lowest energy transition as **H_2tpda**. The $S_0 \rightarrow S_3$ transition of CP linkers corresponds to the $S_0 \rightarrow S_7$ transition of the dimers, increasing the 2PA cross-section up to 3.7 GM. This 2PA active transition has a mixed CT and local exciton (LE) character (see Table S7, Supporting Information), with the electronic contribution originating from both molecules in the dimer, as depicted in Figure 3b. The observed increase in 2PA cross-sections is dominated by intermolecular CT, which enhances the electronic coupling between neighboring **tpda** molecules. Although both the $S_0 \rightarrow S_3$ and $S_0 \rightarrow S_4$ transitions are CT-based for the dimers (see Table S7, Supporting Information), slight differences in molecular orientation and electronic coupling lead to variations in the spectral changes. For example, the cross-section of the $S_0 \rightarrow S_3$ transition in one dimer is 1.4 GM, while in the other, it is 0.05 GM (Figure 3b). This observation arises from the differing strengths of electronic coupling in the stacked molecules. In a CP measured experimentally, the contributions from different neighbouring linkers and their assemblies, with slightly varied local contributions and interactions, couple together, enhancing the overall 2PA effect in **Zntpda**.

The interaction energy between two **tpda** molecules in a dimer is 30.21 kcal mol^{-1} and 31.60 kcal mol^{-1} for **dimer A** and **dimer B**, respectively, highlighting the significant role of intermolecular forces in facilitating CT, which is crucial for the enhanced nonlinear optical response. It is relatively strong and does not differ much from the interaction energy reported previously for different planar PDI aggregates.[36] The noncovalent interaction index (NCI) analysis has been performed to understand the spatial differences and strengths of the intermolecular interactions. It is based on analyzing the electron density and its distribution within the molecular system.[37] The low-density regions between the interacting molecules, which correspond to non-covalent interactions, are revealed by calculating the reduced density gradient (RDG). The visualization of RDG, i.e. the presence of intermolecular interactions between **tpda** in its dimers extracted from **Zntpda**, is demonstrated by green surfaces in **Figure 4**. They differ in the case of both dimer types, indicating weakened van der Waals (vdW) interactions and pronounced C—H···π bonding on the rather short interatomic distance of ≈ 3.03 Å for **dimer A**. At the same time, the aggregation type in **dimer B** clearly shows the preference for π-stacking and vdW interactions. The interaction distance in this case is ≈ 3.57 Å (Figure 4b). The slight change in the type of intermolecular forces is also denoted by the NCI plot, where the reduced density gradient (s) attains low values (down-pointing spikes) more densely in the electron density range of 0–0.005 a.u., where vdW forces are typically described.[37]

The impact of intermolecular interactions is also visible in the slight changes in the character of 2PA-involved orbital

Table 1. MPA values of **Zntpda** were determined by Z-scan.

2PA Wavelength [nm]	2PA Coefficient [cm/GW]	2PA cross-section [GM]	3PA Wavelength [nm]	3PA Coefficient [cm^3/GW^2]	3PA cross-section [$1e^{-74}$ cm^6 s^2 $photon^{-2}$ $molecule^{-1}$]
700	27	29939 ± 1497	**860**	5.7	1.19 ± 0.06
710	23.4	25582 ± 1279	**870**	6.6	1.34 ± 0.07
720	10	10780 ± 539	**880**	7.2	1.43 ± 0.07
730	58.4	62095 ± 3105	**890**	7	1.36 ± 0.07
740	46	48250 ± 2413	**900**	30	5.71 ± 0.29
750	44	45537 ± 2277	**910**	25.8	4.80 ± 0.24
760	46	46980 ± 2349	**920**	26	4.74 ± 0.24
770	50	50402 ± 2520	**930**	27	4.81 ± 0.24
780	51	50751 ± 2538	**940**	29	5.06 ± 0.25
790	51	50109 ± 2505	**950**	28	4.78 ± 0.24
800	17.2	16688 ± 834			
810	22	21082 ± 1054			
820	25	23664 ± 1183			
830	25	23379 ± 1169			
840	25.2	23286 ± 1165			
850	25.6	23377 ± 1169			

transitions as depicted in Figure 3b. Here, the electron density change upon the excitation is shown in blue for electron-deficient regions, which donate the electron density to the accepting regions (marked in green), indicating the electron-rich character of the latest after light absorption. Higher electron density delocalization between the molecules is visible for $S_0 \rightarrow S_7$ of dimer A, corresponding to the transition from the HOMO-4 to the LUMO orbital (46%). This transition has a mixed character for dimer B, where the transition from the HOMO-5 to LUMO orbital (31%) occurs in addition (Figure S23, Supporting Information). The

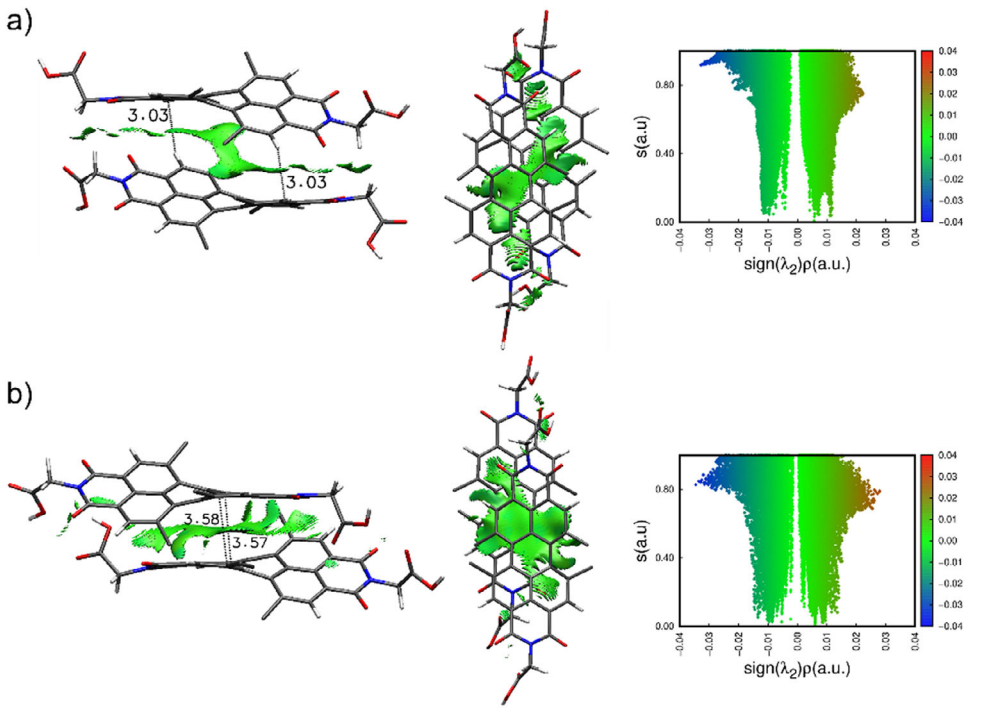

Figure 4. The visualization of the noncovalent interactions (in green, isovalue of RDG of 0.3 a.u.) between **tpda** in **dimer A** (a) and **dimer B** (b) extracted from the CP crystal. Two visualization views for each case are depicted with the NCI plots, representing the relationship between the RDG (*s*) and the sign of the second eigenvalue (λ_2) of the promolecular density. The lower the *s*, the stronger the interaction. Typical van der Waals interactions are described by $\rho < 0.005$ a.u., while attractive interactions, e.g., due to H-bonds, correspond to the negative sign of $0.005 < \rho < 0.05$ a.u.

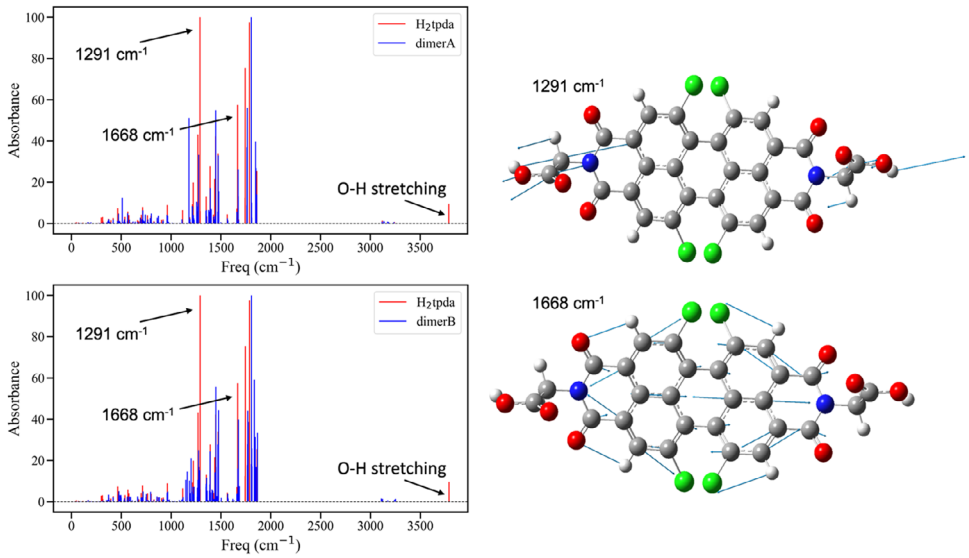

Figure 5. IR spectrum of the **H_2tpda** linker in comparison to IR spectra of **dimer A** (left top) and **dimer B** (left bottom). Optimized structures in the S_0 state have been considered. The visualization of vibrational modes of **H_2tpda** (represented by green arrows) with the frequency of 1291 cm^{-1} and 1668 cm^{-1} is depicted in the right panel.

transition orbitals corresponding to $S_0 \rightarrow S_3$ also show slight differences. The presence of intermolecular CT between species is visible, as shown by the detailed analysis of CT characteristics explained in SI (Figure S23 and Table S7, Supporting Information). Thus, the enhancement of $\sigma^{(2)}$ in **Zntpda** is attributed to incorporating 2PA-active **H_2tpda** into the framework. In such a case, the possibility of conformational locking may additionally enhance $\sigma^{(2)}$. As reported by Zeman et al., such structural effects may dominate 2PA responses modulated by typical H-aggregation, which often weakens the 2PA cross-section.[18a,22d]

To estimate the change in the vibrational flexibility of **H_2tpda** after its assembly in CP, the vibrational modes of the isolated linker and the dimers extracted from the MOF have been analyzed. From the data presented in **Figure 5**, it is visible that some of the vibrational modes are less pronounced in the extracted dimers, particularly for the modes at 1291 cm^{-1} and 1668 cm^{-1}. They involve, to a high extent, the C—O and C═O bonds stretching (see the visualized structural moves represented by arrows in the right panel in Figure 5) and slight breathing motions of the perylene core. From the analysis of the Huang–Rhys factors for **H_2tpda** (see Figure S27, Supporting Information), showing the most dominant changes in the vibrational modes upon reaching the lowest singlet excited state, we see that, among all intense low-frequency vibrations, the one at 1394 cm^{-1} plays an important role in the excited state. It is assigned to the motion of the perylene core, and such an observation agrees with previous experimental and theoretical investigations.[38] Moreover, the spectra calculated satisfactorily reproduce the experimental spectra of **H_2tpda** and **Zntpda** (Figure S6, Supporting Information). Since the carboxyl groups of **H_2tpda** are connected to the SBUs in CPs and the vibrational motions of the perylene cores are altered by the noncovalent interactions with the neighboring linkers, linker vibrations are limited in the CP. Thus, conformational locking enables specific interactions between PDIs in the packing arrangement, which, through electronic coupling and CT-like states, leads to spectral changes and an enhanced 2PA response. The experimentally observed increase in 2PA amounts to a more than three-order-of-magnitude enhancement for **Zntpda**.

Even 3PA can be observed and dominates for excitation wavelengths longer than 850 nm. The measured 3PA cross sections $\sigma^{(3)} = 10^{-74}$ $cm^6s^2photon^{-2}$ are comparatively high for CP-based materials.[18d,39]

3. Conclusion

We synthesized and structurally characterized the zinc-based coordination polymer **Zntpda**, using the PDI-derived chromophore **H_2tpda** as a linker motif. The chromophores in the structure are tightly packed and, after photophysical characterization, were shown to favor H-type aggregation and show no emission. This suggests a high probability of PET, which, in conjecture with H-aggregation, explains the lack of fluorescence in the CP. The results of the DFT and TD-DFT calculations support these conclusions based on the electronic coupling between chromophores.

We investigated both the linker and the CP for their MPA properties. The Z-scan measurements of the CP crystal revealed an increase of three orders of magnitude in $\sigma^{(2)}$ upon incorporating **H_2tpda** into the framework. TD-DFT calculations of dimeric structures mimicking the steric relations in the CP show an approximate increase of 33% per interactive chromophore pair. This substantial increase originates from the induced conformational locking of the species in the MOF framework, coordination with the SBUs, and intermolecular interactions. Altogether, it permits the electronic coupling between organic linkers in the MOF and cooperative effects, enhancing MPA performance.

Our results reveal the potential of PDI-based chromophores in the nonlinear optics of CPs. We demonstrate the significant enhancement of the MPA properties of CPs by orientation and packing of the chromophores, which can be further implemented in related crystalline materials. The findings suggest that the

observed spectral changes are driven by a cooperative interplay of factors such as chromophore chemical composition, molecular orientation, conformational locking, electronic coupling, and intermolecular interactions. Due to the highly adaptive potential of CP and MOF materials, tailoring the chromophore aggregation and photophysical behavior in molecular crystals is an attractive concept for the fabrication of new functional materials. However, more systems are required to study that would consequently enable comparative investigations that establish structure-property relationships contributing to the discovery of design principles for MOFs and CPs in potential NLO-based applications.[22b,d,23,40] Specifically, we propose to study the substitution effects of different functional groups in the bay region of PDIs and their effect on the MPA capabilities in MOFs and CPs. Another effect worth exploring is the formation of J-type aggregates of PDI chromophores in MOFs to potentially enhance the MPA response.

4. Experimental Section

Materials and Methods: All purchased reagents were received from chemical suppliers and used without any further purification if not otherwise stated. All reactions with air- and moisture-sensitive compounds were carried out under standard Schlenk techniques using Argon 4.6 (Westfalen) or in a glovebox (UNIlab, M. Braun). The required glassware was flame-dried in a vacuum before use. Elemental analysis was performed at the Elemental Analysis Lab of the CRC at the Technical University of Munich. Analysis of C, H, and N values was conducted by the flash combustion method at 1800 °C. NMR spectra were recorded on a Bruker AV400 at room temperature at 400 MHz. Single-crystal X-ray diffraction (SC-XRD) data were collected on a Bruker D8 Venture system equipped with a Mo TXS rotating anode (λ = 0.71073 Å) and a CMOS photon 100 detector (for detailed information, see the Supporting Information). UV/Vis spectra in solution were recorded on a double-beam Lambda 365 UV–Vis spectrophotometer from PerkinElmer. All diffuse reflectance spectra were recorded on a Shimadzu UV-3600 Plus UV–vis-NIR spectrophotometer with an ISR-603 integrating sphere attachment. Powder samples were fixed between two quartz glass slides for measurement. The fluorescence QY was measured with the absolute photoluminescence QY measurement system C11347-12 Quantaurus by Hamamatsu. Capillary PXRD measurements were recorded in transmission geometry on a Panalytical Empyrean instrument. The detection was carried out with a Pixel3D detector. All measurements were performed with Cu–Kα (λ = 1.54 Å) radiation and at 298 K. Fluorescence emission measurements were recorded on an FS5 spectrofluorometer from Edinburgh Instruments in solution (linker) or a PMMA matrix (CPs). IR measurements were conducted on a PerkinElmer Frontier FT-IR spectrometer. Multiphoton excitation spectra of CPs were performed using a femtosecond-oscillator-based Z-scan setup designed previously.[35a] Broadband two-photon excitation spectra of linker molecules were recorded using a home-built setup based on a non-collinear optical parametric amplifier and a common-path birefringent interferometer.[41]

Synthesis: *1,6,7,12-tetrachloro-perylene-3,4,9,10-tetracarboxylic anhydride*. The synthesis was performed according to a literature-known synthesis.[42] In a Schlenk flask flushed with argon, 1.00 g of perylene-3,4,9,10-tetracarboxylic acid anhydride (2.50 mmol, 1.00 equiv.) and 0.17 g of iodine (0.68 mmol, 0.27 equiv.) in 6.55 mL of chlorosulfonic acid were stirred for 2 days at 70 °C. After completion of the reaction, the reaction mixture was slowly poured onto ice water. The precipitating orange solid was filtered, washed with water, and dried (1.32 g, 2.49 mmol, 99%).

^{1}H NMR (400 MHz, $CDCl_3$, δ): 8.74 (s, 4H, Ar-H)

1,6,7,12-tetrachloroperylenediimide-N,N'-di-(acetic acid) (***H_2tpda***). The synthesis was performed with a modified literature synthesis.[43] For the synthesis of the linker H_2tpda, 1.00 g of 1,6,7,12-tetrachloro-perylene-3,4,9,10-tetracarboxylic anhydride (1.89 mmol, 1.0 equiv.) was added to 2.83 g glycine (37.7 mmol, 20 equiv.) and dissolved in 50.0 mL propionic acid. The red reaction mixture was stirred at 160 °C for 48 h. Subsequently, the obtained suspension was given to 200 mL distilled water, filtered, and washed with two times 100 mL MeOH/H_2O and 20.0 mL MeOH. The achieved powder was dried in an oven at 100 °C overnight. The product was obtained as a dark red powder with a yield of 84% (1.02 g, 1.59 mmol).

^{1}H NMR (400 MHz, DMSO-d_6, δ): 13.27 (s, 2H, COOH), 8.67 (s, 4H, Ar-H), 4.80 (s, 4H, CH_2); Anal. calcd. for $C_{28}H_{10}Cl_4N_2O_8$: C, 52.21; H, 1.56; N, 4.35. Found: C, 52.06; H, 1.37; N, 4.34.

[Zn_2tpda(DMA)$_2$(DMF)$_{0.3}$] (***Zntpda***) A solution of 13.9 mg $Zn(NO_3)_2$ (3 equiv.) in 1.00 mL DMF was added to a solution of 10.0 mg **H_2tpda** (1 equiv.) in 2.00 mL DMF and put into an oven at 120 °C for 48 h. Subsequently, the afforded solid was filtered, washed with DMF, and dried on air. The product **Zn(tpda)** was obtained as dark red crystals.

Anal. calcd. for $ZnC_{32.9}H_{22.1}Cl_4N_{4.3}O_{8.3}$: C, 44.75; H, 2.52; N, 6.82. Found: C, 45.45; H, 2.48; N, 6.11.

Computational Details: The ground state (S_0) and the first excited singlet state (S_1) geometries of **H_2tpda** were optimized at the time-dependent (TD)-density functional theory (DFT) level with the CAM-B3LYP functional[44] employing the Grimme's D3-dispersion correction with Becke-Johnson damping (D3(BJ))[45] and def2-TZVP basis set[46] in *implicit* tetrahydrofuran (THF) using polarizable continuum model (PCM).[47] The structures obtained are depicted in Figure S20 (Supporting Information). Vibrational analysis was conducted upon all optimizations. Similar calculations were performed for the two dimer structures extracted from the crystal structure of **Zntpda** (see Figures S15 and S20, Supporting Information). However, the optimization of dimers was performed in the gas phase by freezing the oxygen (and saturated with hydrogen) atoms to mimic the structural confinement of linkers in CP. In addition to confirming the correctness of the minima obtained, a vibrational analysis was conducted. All calculations mentioned were conducted in Gaussian16 Rev. C. 01 with convergence criteria of 10^{-8} Hartree and an ultrafine grid.[48]

One-photon absorption (1PA)[49] and two-photon absorption (2PA)[50] spectra were computed for **H_2tpda** using *implicit* THF employing the conductor-like screening model (COSMO) and dimeric systems (**dimer A** and **dimer B**) in the gas phase using TD-CAM-B3LYP-D3(BJ)/def2-TZVP in TURBOMOLE Version 7.5.[51] The calculation of all spectra was performed starting from the respective optimized ground state geometry. The Resolution of the Identity (RI) approximation and an energy convergence criterium of 10^{-8} Hartree were used. 2PA spectra were calculated considering a single laser beam with linearly polarized light and parallel polarization, matching the experimental set-up and following the approach of by Beerepoot et al.[52] Two photons of the same frequency were considered for the calculation of transition moments. Spectra were plotted using half width at half maximum (HWHM) of 0.1 eV and a Lorentzian type broadening function. The macroscopic 2PA cross sections, $\sigma^{(2)}$, were calculated as:

$$\left\langle \sigma^{2PA} \right\rangle = \frac{N\pi^2 \alpha {a_0}^5 \omega^2}{c} \left\langle \delta^{2PA} \right\rangle g\left(2\omega, \omega_0, \Gamma\right) \quad (1)$$

where N is equal to 4, α is the fine structure constant, α_0 is the Bohr radius, ω is the photon energy in atomic units, c is the speed of light, $<\delta_{2PA}>$ is the rotationally averaged 2PA strength and $g(2\omega,\omega_0,\Gamma)$ is the lineshape function related to spectral broadening effects. The rotationally averaged 2PA strength (in atomic units), $<\delta_{2PA}>$, was obtained according to:

$$\left\langle \delta^{2PA} \right\rangle = \frac{1}{15}\left(2\sum_{a,b} S_{ab}S_{ab}^{*} + \sum_{a,b} S_{aa}S_{ab}^{*}\right) \quad (2)$$

where the S_a and S_b are the Cartesian components of the transition moments (S).

Vibrationally resolved spectra were calculated employing the Frank–Condon (FC)[53] approximation with linear coupling model (LCM) approach (TD-FC-LCM)[54] using Dynavib[55] and plotted with half width at half maximum (HWHM) of 0.02 eV and Lorentzian type broadening function. Both time-dependent (TD) and time-independent (TI) approaches were utilized. *Implicit* THF (PCM model) environment was applied for

H_2tpda, while the gas-phase calculations were performed for the dimers. All calculations were performed using the optimized ground state and excited state geometries. The IR spectra were computed utilizing the vibrational frequencies generated upon geometry optimizations to study vibrational modes of all molecular systems.

The hole and electron analysis was computed employing the Multiwfn (version 3.6) analyzer.[56] The electronic coupling between molecules in the optimized dimer structures was calculated using the direct coupling approach.[57]

Finally, the interaction energy between linkers upon CP formation was estimated using a single-point calculation of the optimized dimers and the monomers in that precise geometry according to:[36]

$$E_{interaction} = E_{dimer} - (2 \cdot E_{monomer}) \quad (3)$$

[CCDC 2404573 contains the supplementary crystallographic data for this paper. These data can be obtained free of charge from The Cambridge Crystallographic Data Centre via www.ccdc.cam.ac.uk/data_request/cif.]

Supporting Information

Supporting Information is available from the Wiley Online Library or from the author.

Acknowledgements

This research was funded by the Deutsche Forschungsgemeinschaft (DFG) via SPP 1928 COORNETs and within the frame of the EXC 2089 Cluster of Excellence. The authors acknowledge support by the state of Baden-Württemberg through bwHPC and the DFG through Grant No. INST 40/575-1 FUGG (JUSTUS 2 cluster) under project bw20F004. Financed by the Ministry of Science, Research and the Arts of Baden-Württemberg as part of the sustainability financing of the projects of the Excellence Initiative II. The TUM is very greatly acknowledged for institutional funding. S.N.D., S.J.W., and Y.C. thank the TUM Graduate School for financial support. Y.C. would like to thank Franziska Chalupa-Gantner for measurement support.

Open access funding enabled and organized by Projekt DEAL.

Conflict of Interest

The authors declare no conflict of interest.

Data Availability Statement

The data that support the findings of this study are available in the supplementary material of this article.

Keywords

coordination polymers, multiphoton absorption, nonlinear optics, structure–property relationships

Received: December 13, 2024
Revised: April 10, 2025
Published online:

[1] E. Mattia, S. Otto, *Nat. Nanotechnol.* **2015**, *10*, 111.
[2] F. J. M. Hoeben, P. Jonkheijm, E. W. Meijer, A. P. H. J. Schenning, *Chem. Rev.* **2005**, *105*, 1491.
[3] F. Würthner, C. R. Saha-Möller, B. Fimmel, S. Ogi, P. Leowanawat, D. Schmidt, *Chem. Rev.* **2016**, *116*, 962.
[4] F. Zhang, Y. Ma, Y. Chi, H. Yu, Y. Li, T. Jiang, X. Wei, J. Shi, *Sci. Rep.* **2018**, *8*, 8208.
[5] Y. Guo, Z. Ma, X. Niu, W. Zhang, M. Tao, Q. Guo, Z. Wang, A. Xia, *J. Am. Chem. Soc.* **2019**, *141*, 12789.
[6] T. A. Barendt, L. Ferreira, I. Marques, V. Félix, P. D. Beer, *J. Am. Chem. Soc.* **2017**, *139*, 9026.
[7] S. E. Penty, M. A. Zwijnenburg, G. R. F. Orton, P. Stachelek, R. Pal, Y. Xie, S. L. Griffin, T. A. Barendt, *J. Am. Chem. Soc.* **2022**, *144*, 12290.
[8] P. D. Frischmann, V. Kunz, F. Würthner, *Angew. Chem., Int. Ed.* **2015**, *54*, 7285.
[9] X. Shang, I. Song, J. H. Lee, J. C. Kim, H. Ohtsu, W. Choi, J. Ahn, K. Gao, M. Zhang, M. Kawano, S. K. Kwak, J. H. Oh, *Adv. Opt. Mater.* **2023**, *11*, 2300534.
[10] Z. Liu, C. Li, J. Chen, X. Li, F. Luo, F. Cheng, J.-J. Liu, *Inorg. Chem. Front.* **2022**, *9*, 111.
[11] B. Lü, Y. Chen, P. Li, B. Wang, K. Müllen, M. Yin, *Nat. Commun.* **2019**, *10*, 767.
[12] P. I. Scheurle, A. Biewald, A. Mähringer, A. Hartschuh, D. D. Medina, T. Bein, *Small Struct.* **2022**, *3*, 2100195.
[13] H. J. Park, M. C. So, D. Gosztola, G. P. Wiederrecht, J. D. Emery, A. B. F. Martinson, S. Er, C. E. Wilmer, N. A. Vermeulen, A. Aspuru-Guzik, J. F. Stoddart, O. K. Farha, J. T. Hupp, *ACS Appl. Mater. Interfaces* **2016**, *8*, 24983.
[14] J.-J. Li, S.-Y. Liu, G. Liu, Y.-G. Liu, G.-Z. Wu, H.-D. Li, R. Krishna, X.-Q. Liu, L.-B. Sun, *Sep. Purif. Technol.* **2023**, *320*, 124109.
[15] S. N. Deger, S. J. Weishäupl, A. Pöthig, R. A. Fischer, *Energies* **2022**, *15*, 2437.
[16] L. Wang, Y.-L. Liu, Q.-J. Li, S.-H. Chen, D. He, M.-S. Wang, *J. Phys. Chem. A* **2022**, *126*, 870.
[17] S. J. Weishäupl, D. C. Mayer, Y. Cui, P. Kumar, H. Oberhofer, R. A. Fischer, J. Hauer, *J. Mater. Chem. C* **2022**, *10*, 6912.
[18] a) R. Medishetty, J. K. Zaręba, D. Mayer, M. Samoć, R. A. Fischer, *Chem. Soc. Rev.* **2017**, *46*, 4976; b) S. J. Weishäupl, Y. Cui, S. N. Deger, H. Syed, A. Ovsianikov, J. Hauer, A. Pöthig, R. A. Fischer, *Chem. Mater.* **2022**, *34*, 7402; c) N. Liu, Z. Chen, W. Fan, J. Su, T. Lin, S. Xiao, J. Meng, J. He, J. J. Vittal, J. Jiang, *Angew. Chem., Int. Ed.* **2022**, *61*, 202115205; d) H. S. Quah, W. Chen, M. K. Schreyer, H. Yang, M. W. Wong, W. Ji, J. J. Vittal, *Nat. Commun.* **2015**, *6*, 7954.
[19] L. S. Lancaster, T. D. Krueger, C. Chen, E. N. Musa, J. M. Lessard, N.-C. Chiu, M. T. Nord, K. C. Stylianou, *Chem. Phy. Rev.* **2024**, *5*, 021401.
[20] a) C. Lu, J. Yu, H. Sheng, Y. Jiang, F. Zhao, J. Wang, *Nanomaterials* **2022**, *12*, 535; b) S. Sanyal, A. Painelli, S. K. Pati, F. Terenziani, C. Sissa, *Phys. Chem. Chem. Phys.* **2016**, *18*, 28198; c) L. Sun, W. Zhu, W. Wang, F. Yang, C. Zhang, S. Wang, X. Zhang, R. Li, H. Dong, W. Hu, *Angew. Chem., Int. Ed.* **2017**, *56*, 7831.
[21] D. C. Mayer, A. Manzi, R. Medishetty, B. Winkler, C. Schneider, G. Kieslich, A. Pöthig, J. Feldmann, R. A. Fischer, *J. Am. Chem. Soc.* **2019**, *141*, 11594.
[22] a) A. Justyniarski, J. K. Zaręba, P. Hańczyc, P. Fita, M. Chołuj, R. Zaleśny, M. Samoć, *J. Mater. Chem. C* **2018**, *6*, 4384; b) S. Biswas, H.-Y. Ahn, M. V. Bondar, K. D. Belfield, *Langmuir* **2012**, *28*, 1515; c) S.-J. Chung, K.-S. Kim, T.-C. Lin, G. S. He, J. Swiatkiewicz, P. N. Prasad, *J. Phys. Chem. B* **1999**, *103*, 10741; d) C. J. I. V. Zeman, G. Kang, K. L. Kohlstedt, *ACS Appl. Mater. Interfaces* **2022**, *14*, 45644.
[23] I. F. A. Mariz, S. Raja, T. Silva, S. Almeida, É. Torres, C. Baleizão, E. Maçôas, *Dyes Pigm.* **2021**, *193*, 109470.
[24] V. A. Blatov, A. P. Shevchenko, D. M. Proserpio, *Cryst. Growth Des.* **2014**, *14*, 3576.
[25] I. Solymosi, C. Neiß, H. Maid, F. Hampel, T. Solymosi, A. Görling, A. Hirsch, M. E. Pérez-Ojeda, *ChemistrySelect* **2023**, *8*, 202300523.
[26] a) Z. Chen, V. Stepanenko, V. Dehm, P. Prins, L. D. A. Siebbeles, J. Seibt, P. Marquetand, V. Engel, F. Würthner, *Chem. - Eur. J.* **2007**, *13*,

436; b) A. Oleson, T. Zhu, I. S. Dunn, D. Bialas, Y. Bai, W. Zhang, M. Dai, D. R. Reichman, R. Tempelaar, L. Huang, F. C. Spano, *J. Phys. Chem. C* **2019**, *123*, 20567.
[27] S. Ma, S. Du, G. Pan, S. Dai, B. Xu, W. Tian, *Aggregate* **2021**, *2*, 96.
[28] M. Adams, M. Kozlowska, N. Baroni, M. Oldenburg, R. Ma, D. Busko, A. Turshatov, G. Emandi, M. O. Senge, R. Haldar, C. Wöll, G. U. Nienhaus, B. S. Richards, I. A. Howard, *ACS Appl. Mater. Interfaces* **2019**, *11*, 15688.
[29] a) X. Ma, W. Chi, X. Han, C. Wang, S. Liu, X. Liu, J. Yin, *Chin. Chem. Lett.* **2021**, *32*, 1790; b) B. Xu, C. Wang, W. Ma, L. Liu, Z. Xie, Y. Ma, *J. Phys. Chem. C* **2017**, *121*, 5498; c) L. E. Shoer, S. W. Eaton, E. A. Margulies, M. R. Wasielewski, *J. Phys. Chem. B* **2015**, *119*, 7635.
[30] H. Hashimoto, K. Isobe, A. Suda, F. Kannari, H. Kawano, H. Mizuno, A. Miyawaki, K. Midorikawa, *Appl. Opt.* **2010**, *49*, 3323.
[31] M. Pawlicki, H. A. Collins, R. G. Denning, H. L. Anderson, *Angew. Chem., Int. Ed.* **2009**, *48*, 3244.
[32] a) E. Garoni, F. Nisic, A. Colombo, S. Fantacci, G. Griffini, K. Kamada, D. Roberto, C. Dragonetti, *New J. Chem.* **2019**, *43*, 1885; b) Z. An, S. A. Odom, R. F. Kelley, C. Huang, X. Zhang, S. Barlow, L. A. Padilha, J. Fu, S. Webster, D. J. Hagan, E. W. Van Stryland, M. R. Wasielewski, S. R. Marder, *J. Phys. Chem. A* **2009**, *113*, 5585; c) W. Feng, K. Liu, J. Zang, J. Xu, H. Peng, L. Ding, T. Liu, Y. Fang, *J. Phys. Chem. B* **2021**, *125*, 11540; d) E. Piovesan, D. L. Silva, L. De Boni, F. E. G. Guimaraes, L. Misoguti, R. Zaleśny, W. Bartkowiak, C. R. Mendonca, *Chem. Phys. Lett.* **2009**, *479*, 52.
[33] K. D. Belfield, M. V. Bondar, O. V. Przhonska, K. J. Schafer, *J. Photochem. Photobiol. A* **2002**, *151*, 7.
[34] K. Ahmadzadeh, X. Li, Z. Rinkevicius, P. Norman, R. Zaleśny, *J. Phys. Chem. Lett.* **2024**, *15*, 969.
[35] a) W. Steiger, P. Gruber, D. Theiner, A. Dobos, M. Lunzer, J. Van Hoorick, S. Van Vlierberghe, R. Liska, A. Ovsianikov, *Opt. Mater. Express* **2019**, *9*, 3567; b) M. Sheik-bahae, A. A. Said, E. W. Van Stryland, *Opt. Lett.* **1989**, *14*, 955.
[36] P. Panthakkal Das, A. Mazumder, M. Rajeevan, R. S. Swathi, M. Hariharan, *Phys. Chem. Chem. Phys.* **2024**, *26*, 2007.
[37] a) E. R. Johnson, S. Keinan, P. Mori-Sánchez, J. Contreras-García, A. J. Cohen, W. Yang, *J. Am. Chem. Soc.* **2010**, *132*, 6498; b) J. Contreras-García, E. R. Johnson, S. Keinan, R. Chaudret, J.-P. Piquemal, D. N. Beratan, W. Yang, *J. Chem. Theory Comput.* **2011**, *7*, 625.
[38] D. Ambrosek, H. Marciniak, S. Lochbrunner, J. Tatchen, X.-Q. Li, F. Würthner, O. Kühn, *Phys. Chem. Chem. Phys.* **2011**, *13*, 17649.
[39] R. Medishetty, L. Nemec, V. Nalla, S. Henke, M. Samoć, K. Reuter, R. A. Fischer, *Angew. Chem., Int. Ed.* **2017**, *56*, 14743.
[40] R. Haldar, A. Mazel, M. Krstić, Q. Zhang, M. Jakoby, I. A. Howard, B. S. Richards, N. Jung, D. Jacquemin, S. Diring, W. Wenzel, F. Odobel, C. Wöll, *Nat. Commun.* **2019**, *10*, 2048.
[41] S. N. Deger, Y. Cui, J. Warnan, R. A. Fischer, F. Šanda, J. Hauer, A. Pöthig, *ACS Appl. Opt. Mater.* **2024**, *2*, 1770.
[42] K. Yoshinaga, T. M. Swager, *Synlett* **2018**, *29*, 2509.
[43] C. Addicott, I. Oesterling, T. Yamamoto, K. Müllen, P. J. Stang, *J. Org. Chem.* **2005**, *70*, 797.
[44] T. Yanai, D. P. Tew, N. C. Handy, *Chem. Phys. Lett.* **2004**, *393*, 51.
[45] S. Grimme, S. Ehrlich, L. Goerigk, *J. Comput. Chem.* **2011**, *32*, 1456.
[46] A. Schäfer, H. Horn, R. Ahlrichs, *J. Chem. Phys.* **1992**, *97*, 2571.
[47] R. Improta, V. Barone, G. Scalmani, M. J. Frisch, *J. Chem. Phys.* **2006**, *125*, 54103.
[48] M. J. Frisch, G. W. Trucks, H. B. Schlegel, G. E. Scuseria, M. A. Robb, J. R. Cheeseman, G. Scalmani, V. Barone, G. A. Petersson, H. Nakatsuji, X. Li, M. Caricato, A. V. Marenich, J. Bloino, B. G. Janesko, R. Gomperts, B. Mennucci, H. P. Hratchian, J. V. Ortiz, A. F. Izmaylov, J. L. Sonnenberg, Williams, F. Ding, F. Lipparini, F. Egidi, J. Goings, B. Peng, A. Petrone, T. Henderson, D. Ranasinghe, et al., *Gaussian 16 Revision C.01*, Gaussian, Inc., Wallingford, CT **2016**.
[49] P. Jörgensen, H. J. r. A. Jensen, J. Olsen, *J. Chem. Phys.* **1988**, *89*, 3654.
[50] C. Hättig, O. Christiansen, P. Jörgensen, *J. Chem. Phys.* **1998**, *108*, 8331.
[51] S. G. Balasubramani, G. P. Chen, S. Coriani, M. Diedenhofen, M. S. Frank, Y. J. Franzke, F. Furche, R. Grotjahn, M. E. Harding, C. Hättig, A. Hellweg, B. Helmich-Paris, C. Holzer, U. Huniar, M. Kaupp, A. Marefat Khah, S. Karbalaei Khani, T. Müller, F. Mack, B. D. Nguyen, S. M. Parker, E. Perlt, D. Rappoport, K. Reiter, S. Roy, M. Rückert, G. Schmitz, M. Sierka, E. Tapavicza, D. P. Tew, et al., *J. Chem. Phys.* **2020**, *152*, 184107.
[52] M. T. P. Beerepoot, D. H. Friese, N. H. List, J. Kongsted, K. Ruud, *Phys. Chem. Chem. Phys.* **2015**, *17*, 19306.
[53] a) F. Santoro, A. Lami, R. Improta, J. Bloino, V. Barone, *J. Chem. Phys.* **2008**, *128*, 224311; b) G. Herzberg, E. Teller, *Z. Phys. Chem.* **1933**, *21B*, 410.
[54] a) G. Tian, Y. Luo, *J. Phys. Chem. C* **2014**, *118*, 14853; b) G. Tian, Y. Luo, *Angew. Chem., Int. Ed.* **2013**, *52*, 4814.
[55] G. Tian, S. Duan, W. Hua, Y. Luo, *DynaVib Version 1.0*, Royal Institute of Technology, Sweden **2012**.
[56] T. Lu, F. Chen, *J. Comp. Chem.* **2012**, *33*, 580.
[57] M. Mostaghimi, H. Pacheco Hernandez, Y. Jiang, W. Wenzel, L. Heinke, *Commun. Chem.* **2023**, *6*, 275.